Jari Varje

Simulation of neutral particle fluxes from fast ions in the JET tokamak

School of Science

Thesis submitted for examination for the degree of Master of Science in Technology.

Espoo 22.3.2016

Thesis supervisor:

Prof. Mathias Groth

Thesis advisors:

Dr. Marko Santala

Dr. Taina Kurki-Suonio

Aalto University
School of Science

AALTO UNIVERSITY
SCHOOL OF SCIENCE

ABSTRACT OF THE
MASTER'S THESIS

Author: Jari Varje

Title: Simulation of neutral particle fluxes from fast ions in the JET tokamak

Date: 22.3.2016 Language: English Number of pages: 5+45

Department of Applied Physics

Professorship: Advanced Energy Systems

Supervisor: Prof. Mathias Groth

Advisors: Dr. Marko Santala, Dr. Taina Kurki-Suonio

Neutral particle analysis (NPA) is a diagnostic method for measuring neutral particle fluxes resulting from charge exchange reactions between neutrals and ions in tokamak plasmas. The neutral atoms can escape the plasma, directly conveying information on the density and temperature of the initial ions. This piece of information in turn is crucial for the upcoming JET D-T campaign as well as eventual fusion reactor operation, where precise control of the ratio of different fuel isotopes is required.

The measured neutral particle fluxes are, however, distorted by energetic particles such as those resulting from neutral beam injection (NBI) heating. The fluxes from the slowing down beam ions mask the signal from the bulk plasma. This complicates analysis of the main plasma ions, while at the same time providing an opportunity to diagnose the injected ions themselves. This can be used to infer properties of the NBI ion distribution as well as determine possible residual isotopic composition of the beams.

In this thesis, the fast ion orbit following code ASCOT, together with other plasma codes available within the JET modelling suite, were used for predictive and interpretive modelling of the distribution and neutral flux of NBI ions in the JET tokamak. The NPA signal was found to be highly dependent on factors such as neutral particle distribution, plasma density and heating scheme, necessitating detailed numerical modelling.

Keywords: fusion, neutral particle analysis, neutral beam injection, JET, ASCOT

AALTO-YLIOPISTO
PERUSTIETEIDEN KORKEAKOULU

DIPLOMITYÖN
TIIVISTELMÄ

Tekijä: Jari Varje

Työn nimi: Nopeiden ionien tuottaman neutraalien hiukkasten vuon simulointi JET-tokamakissa

Päivämäärä: 22.3.2016 Kieli: Englanti Sivumäärä: 5+45

Teknillisen fysiikan laitos

Professuuri: Energiatieteet

Työn valvoja: Prof Mathias Groth

Työn ohjaajat: TkT Marko Santala, TkT Taina Kurki-Suonio

Fuusioplasman polttoaineiden seossuhteen määrittäminen ja hallinta on keskeistä tulevaisuuden fuusioreaktoreille. Neutraalien hiukkasten analysointi (neutral particle analysis, NPA) on diagnostiikkamenetelmä, jossa mitataan tokamak-reaktorin plasman emittoimien atomien vuota. Koska nämä hiukkaset ovat varauksettomia, ne voivat paeta tokamakin koossapitävästä magneettikentästä, ja mitatun vuon avulla voidaan määrittää plasman koostumus.
Suurienergiset hiukkaset, kuten plasman kuumentamiseen käytettävistä neutraalisuihkuista (neutral beam injection, NBI) syntyvät ionit, voivat hidastuessaan vääristää plasman varauksettomien hiukkasten vuota. Tämä vaikeuttaa plasman termisten polttoaineionien mittaamista, mutta toisaalta mahdollistaa itse neutraalisuihkujen tuottaman nopeiden ionien jakauman ja koostumuksen diagnosoinnin.
Tässä diplomityössä suurienergisten hiukasten radanseurantakoodia ASCOTia sekä joukkoa muita plasmasimulaatiokoodeja käytettiin sekä tulkitseviin että ennustaviin NBI-hiukkasten NPA-simulaatioihin JET-tokamakissa. NPA-signaalin havaittiin riippuvan voimakkaasti neutraalien hiukkasten jakaumasta, plasman tiheydestä sekä käytetystä kuumennusmenetelmästä.

Avainsanat: fuusio, NPA, NBI, JET, ASCOT

Contents

1 Introduction

Nuclear fusion is a promising energy production method for the future. Consuming abundant fuels, and producing no carbon dioxide emissions and little long-term radioactive waste, it is an attractive alternative to conventional energy sources.

1.1 Nuclear fusion and tokamaks

Nuclear fusion is based on the nuclear reactions where two light nuclei fuse into heavier elements. The easiest reaction to achieve, yielding the highest fusion output at the lowest temperature, is the fusion of deuterium and tritium, the two heavier hydrogen isotopes. The reaction

$$^2D +^3 T \rightarrow ^4He(3.5MeV) + n(14.1MeV) \quad (1)$$

consumes one deuteron and one triton, producing a 3.5 MeV alpha particle and a 14.1 MeV neutron in the process. Temperatures on the order of one hundred million Kelvins, or 10 keV, are required in order for the positively charged nuclei to overcome the Coulomb repulsion between them. At these temperatures the fusion fuel is a plasma composed of charged particles.

In order to produce fusion power, the high temperature plasma must be confined sufficiently long for the fusion reactions to take place. The leading method for this is the tokamak, where the plasma is confined using magnetic fields. A helical magnetic field is created using a set of external coils and a current running through the plasma (figure 1). This configuration results in concentric closed flux surfaces inside the plasma extending from the center of the plasma through to the last closed flux surface (LCFS) or separatrix, where after the field lines are in contact with the device walls (figure 2). The plasma within the separatrix is called the core plasma. Edge plasma is the region just inside the separatrix, typically encompassing approximately 5-10% of the minor radius of the plasma. Plasma in contact with the wall outside the separatrix is called the scrape-off layer (SOL).

The charged particles in the plasma are restricted to follow the magnetic field lines, orbiting them due to the Lorentz force. Because of this the particles can easily move along the field lines, while cross-field transport is con-

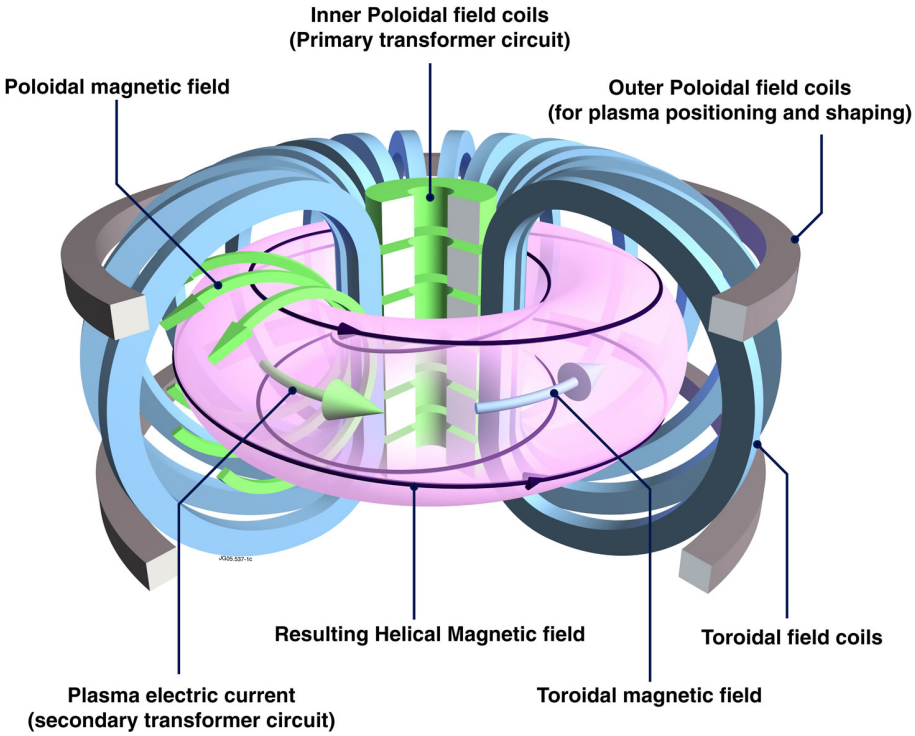

Figure 1: Schematic of tokamak magnetic fields and field coils. [1]

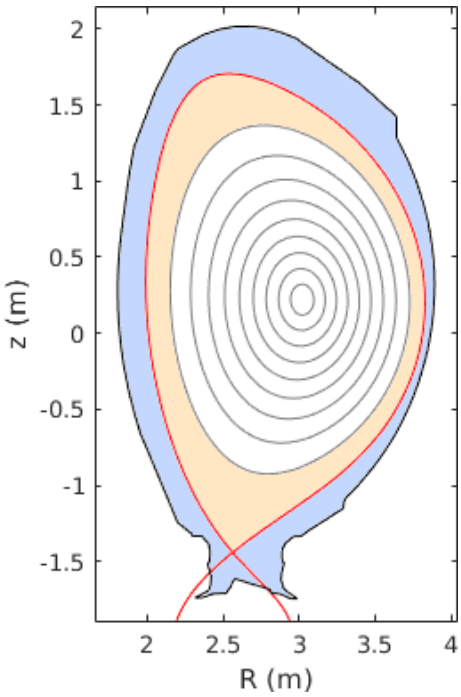

Figure 2: Poloidal view of a tokamak plasma with flux surfaces in the core drawn in grey and the separatrix in red. The edge plasma is depicted with orange color and the scrape-off layer in blue.

strained. Thus, the plasma can be described through one dimensional density and temperature profiles as a function of normalized radial coordinate $\rho_{\mathrm{pol}} = \sqrt{(\psi - \psi_{\mathrm{axis}})/(\psi_{\mathrm{sep}} - \psi_{\mathrm{axis}})}$, where ψ_{axis} and ψ_{sep} are the poloidal fluxes at the center of the plasma and the separatrix, respectively. The plasma parameters are assumed to remain constant on each flux surface. [2]

1.2 Fuel isotope ratio and diagnostics

For optimum burn, precise control of the relative densities of the fuel isotopes in the plasma is required, as any excess of one isotope dilutes the plasma for the other isotope and reduces fusion performance. [3] Thus controlling the fuel mixture is of paramount importance for efficient reactor operation, and this in turn requires precise measurement of the ratio of the two fuel isotopes.

Diagnosing ions deep inside the core plasma is, however, very challenging. Relative ion densities can be inferred through Balmer alpha spectroscopy, which measures the radiation emitted by neutralized ions. Distinguishing different isotopes of hydrogen based on spectral lines is, however, difficult due to the close proximity of D_α and T_α emission lines. [4] The measurements can also be performed in the scrape-off layer, where the temperature is lower and atomic hydrogen isotopes are more abundant. This method, however, only yields the fuel ratio in the SOL, which may not correspond to the ratio in the core. [5] The isotope ratio can also be estimated indirectly by measuring the energy spectrum of neutrons, which corresponds to the fusion reaction rates between the different isotopes, and can thus be used to infer the isotope ratio, but this is challenging due to the large differences in the reaction rates. [6]

The best method of measuring the ratio between the isotopes would naturally be directly measuring the actual density of particles. While the ions are confined inside the plasma by the magnetic field, neutral atoms resulting from processes such as recombination or charge exchange can escape the plasma and be measured with the diagnostic method called neutral particle analysis (NPA). The relative fluxes of the two isotopes then correspond to the ratio of the fuel isotopes inside the plasma.

1.3 Fast ion neutral particle analysis

While the principle behind this measurement is simple, in practice many features essential to high performance plasma operation make it difficult to interpret the results. The measured signal represents the total neutral emissions along the detector sight line. As the neutral emissions are produced in charge exchange reactions with existing neutral particles in the plasma, the measured flux depends strongly on the distribution of neutral sources inside the plasma. Additionally, processes such as external heating that only affects one isotope can distort the measured signal. Neutral fluxes from slowing-down high-energy particles can mask the weak signal from the high-energy tail of the thermal or bulk plasma, preventing accurate determination of the relative plasma ion densities.

One such heating method is neutral beam injection (NBI), in which high-energy neutral particles are used to deposit energy and momentum in the plasma for the purposes of heating and current drive. The beams are typically composed of the same particle species as the plasma itself, and thus can distort the ion distribution and resulting neutral particle energy spectrum. On the other hand, the high energy neutral emissions can be used to infer properties of the beam ions themselves.

NPA diagnostics have previously been used to determine the isotope ratio at the JET tokamak with some limited simulations for the NBI neutral fluxes [7, 8]. Some of the tools used in this study have also previously been used for simulating neutral fluxes from beam ions in experiments at the ASDEX Upgrade tokamak [9, 10]. In [10], for some NBI configurations, good agreement between simulations and measurements was found, but for some the agreement was found lacking. This discrepancy was primarily attributed to the limited neutral density source model used in the simulations. Neutral particle analysis, with particular attention to NBI-generated neutrals, has also been studied at ASDEX Upgrade [11].

In this work the synthetic NPA diagnostic ASCOT-NPA is introduced and used, together with a suite of other simulation codes, to simulate the neutral fluxes from NBI ions at the JET tokamak, with the goal of assessing the feasibility of using this approach to improve isotope ratio measurements. Additionally, the simulations are used to study the effect of different NBI heating configurations on the fast ion distribution and the corresponding neutral flux.

The second chapter describes the neutral particle physics relevant to NPA as well as the JET KR2 NPA diagnostic. The third chapter discusses the different sources of neutral particles in a tokamak plasma. The fourth chapter describes the codes used in this study to model the fast ion and neutral distributions and the neutral particle flux. The fifth chapter presents both interpretive as well as predictive results for the fluxes in different plasmas. Finally, the sixth chapter discusses the results and their applications to future studies at JET.

2 Neutral particle analysis

Neutral particle analysis is a diagnostic method for determining the neutral particle emissions from the plasma. As neutral particles are not affected by the magnetic fields, they can carry information of conditions throughout the plasma. However, many other physics processes affect the production and transmission of neutrals in a plasma.

2.1 Atomic reactions in a plasma

Neutral hydrogen atoms can undergo various reactions with charged plasma particles. The most important reactions are the charge-exchange, ion and electron impact ionization processes

$$H^0 + H^+ \longrightarrow H^+ + H^0 \tag{2}$$

$$H^0 + H^+ \longrightarrow H^+ + e^- + H^+ \tag{3}$$

$$H^0 + e^- \longrightarrow H^+ + e^- + e^-. \tag{4}$$

In the charge exchange reaction (1) the neutral atom encounters an ion. The electron orbiting the neutral atom can switch its host and neutralize the incoming ion, causing the original neutral to become charged in the process. While the reaction appears symmetric, the original neutral and ion can have very different energies. Beam ions can have energies of more than 100 keV, while the neutrals inside the plasma range from 1-10 keV for the core plasma to just 1-10 eV for neutrals near the edge of the plasma. In this case the charge exchange reaction effectively interchanges the energy of the neutral and the ion.

Ion impact ionization (2) is a competing process with charge exchange. In this reaction, the energy of the collision between the ion and the neutral atom strips the electron from its host, effectively resulting in a net loss of neutral particles. Electron impact ionization (3) is an analogous process to the ion impact ionization, where the impacting projectile is a passing electron, which strips the neutral of its own electron in the collision. This reaction also results in an effective loss of neutrals.

The probability of the reactions can be described by the cross section σ, which

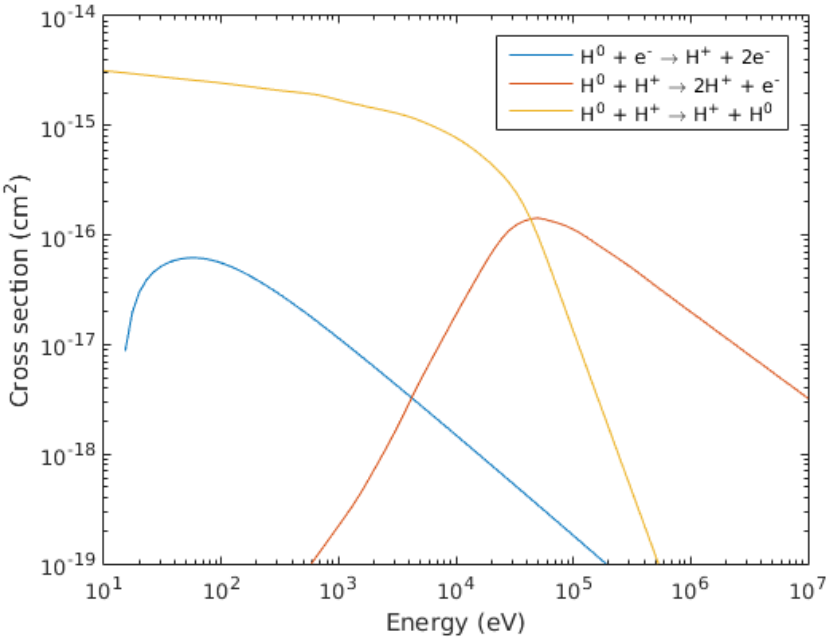

Figure 3: Cross sections as a function of energy for charge exchange, electron impact and ion impact reactions between hydrogen atoms and ions and electrons. [12]

is defined through the reaction rate

$$R = n_0 \Phi \sigma = n_0 n v \sigma \tag{5}$$

where $\Phi = nv$ is the flux of incoming particles at density n and velocity v and n_0 is the density of the second particle species. The probability of the reaction, and thus the cross section, depends on the relative velocity between the two particles. Thus the cross sections can be expressed through rate coefficients $< \sigma v >$ by averaging over the possible velocities

$$< \sigma v >= \int v f(v) \sigma(v) dv \tag{6}$$

where $f(v)$ is the velocity distribution of the particles.

Cross sections for typical charge exchange, electron impact and ion impact processess in fusion plasmas are depicted in figure 3. Charge exchange is the dominant reaction between 1-10 keV, covering the vast majority of current day fusion plasmas. Ion impact ionization becomes relevant above 100 keV, which would be the case for ions accelerated by external heating. Electron

impact ionization, while significant for the temperatures of 100 eV and below encountered near the wall, diminishes above 1 keV, which is a typical inside the core plasma.

2.2 Neutral particle analysis

Neutral particle analysis (NPA) is based on measuring the energy distribution of neutral fluxes emitted by the plasma. Ions inside the plasma are neutralized through charge exchange with existing neutral particles present in the plasma. As they are no longer affected by the confining magnetic field, they can escape the plasma on ballistic trajectories.

As the neutrals travel through the plasma, they can become reionized through the reactions (1-3) and the density of neutrals changes according to the reaction rate

$$\frac{dn_0}{dt} = -nn_e < \sigma v >_i \tag{7}$$

where n is the neutral flux density, n_e is the density of the background plasma and $< \sigma v >_i$ is the ionization rate coefficient. The solution is exponential decay from the source neutral rate S

$$n(s) = Se^{-t/\tau} = Se^{-s/\lambda} \tag{8}$$

where instead of time t and ionization time $\tau = n_e < \sigma v >$ the neutral decay is expressed as a function of distance travelled in the plasma s and the mean free path

$$\lambda = \frac{v}{n_e < \sigma v >} \tag{9}$$

where v is the velocity of the neutrals.[13] As the density and temperature, and thus the ionization cross section, change along the neutral trajectory from the detector to the emission location l, this can be expressed as the integral

$$n(s) = Se^{\int_0^l -s/\lambda ds} \tag{10}$$

The neutral particle analyzer measures the line integrated total of neutrals along its line of sight of length L. The measured flux can then be expressed as the integral

$$\Gamma = \int_0^L S(l)e^{\int_0^l -s/\lambda ds} dl \tag{11}$$

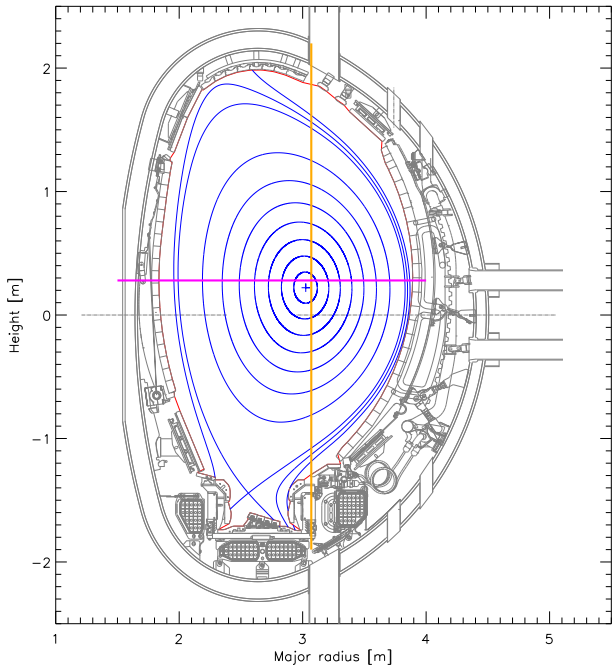

Figure 4: The sight lines of the low-energy NPA diagnostic KR2 (magenta) and the high-energy diagnostic KF1 (orange) at JET.

where the local neutral source is a function of the ion density n_i, neutral density n_0 and charge exchange cross section $< \sigma v >$ and can be expressed as $S = n_i n_0 < \sigma v >_{cx}$. [7]

2.3 Description of the JET KR2 NPA diagnostic

The JET tokamak is outfitted with two NPA diagnostics: the high-energy NPA diagnostic KF1 and the low-energy KR2 neutral particle analyzer/isotope separator (ISEP) (figure 4). The energy range of the high-energy KF1 is too high for diagnosing the NBI ions, and it can only measure single isotopes. The low-energy NPA KR2 is capable of measuring the neutral particle fluxes simultaneously for hydrogen, deuterium and tritium from 1 keV upwards. [14]

The layout of the KR2 NPA diagnostic is depicted in figure 5. The incoming neutral particles are collimated using narrow slits and stripped of electrons by passing them through a 40 nm carbon foil. The resulting ions are then accelerated in up to a 100 kV electric field, which improves the detection efficiency due to the higher energy deposited into the detector. The ions enter the magnet chamber, where a vertical magnetic field is used to deflect the particles 180^o onto the detector. This separates the particles by momentum due

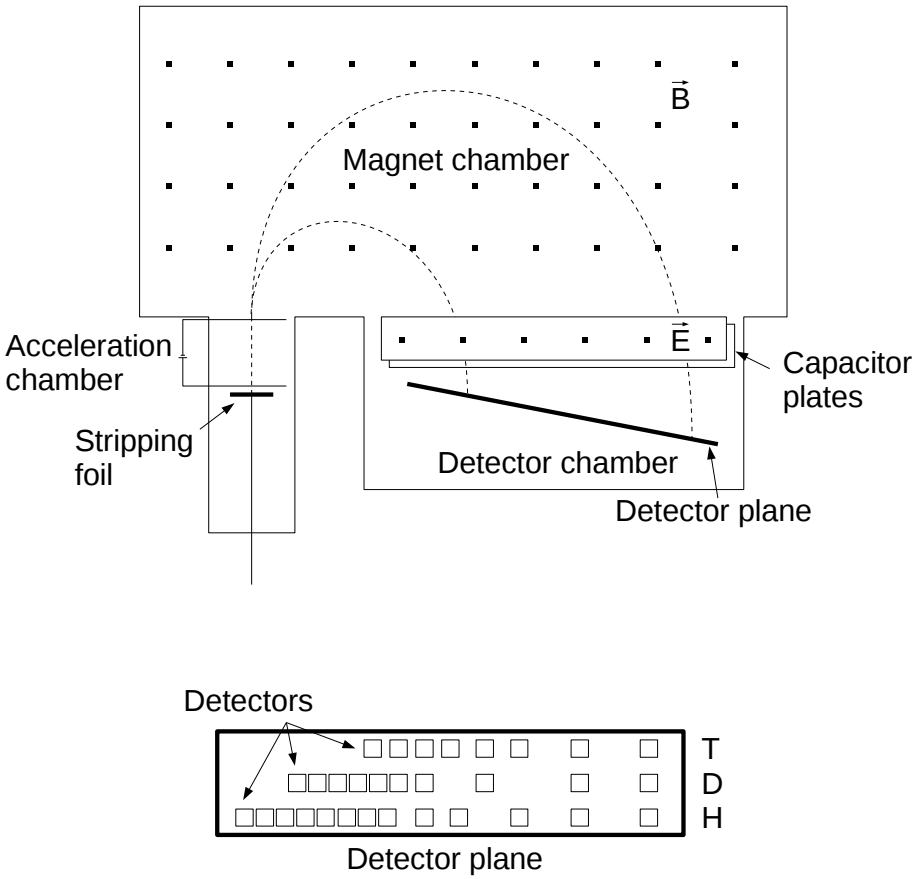

Figure 5: Layout of the JET KR2 NPA diagnostic chambers (top) and the detector plane (bottom).

to the Lorentz force, enabling analysis of their energy distribution. Finally, the ions are passed through an electric field between two capacitor plates, which vertically separates the isotopes with different masses by their velocity.

After becoming separated by the electric and magnetic fields, the ions impact a vertical detector plane, where detectors are positioned in three rows, one for each isotope, at irregular intervals such that the energy of the striking particle can be determined based on the strike point location. The measured energy ranges can be changed by adjusting the strength of the magnetic and electric fields. In this study, the measured energies were 4-97 keV for hydrogen and 5-41 keV for deuterium and 5-22 keV for tritium. The KR2 detectors will be upgraded from traditional CsI scintillators to thin silicon detectors, with low susceptibility to neutron radiation from the fusion reactions [15]. They will also have faster response times and the capability of measuring the energy of the striking particle, which enables separation of particles with identical charge-to-mass ratio such as deuterium and helium-4.

The output of the diagnostic consists of the pulse counts from the analog-to-digital converters (ADC) of the detectors divided into bins based on the energy deposited into the detector (figure 6). The first 19 energy bins are assumed to consist of neutron impacts, which only deposit little energy into the thin detector, while the remaining bins are considered actual signal from the neutral particle flux.

The pulse counts for the background and signal bins are summed to determine total atom and neutron fluxes for each energy channel. The quality of the signal can then be assessed by comparing their relative levels. For example in the case of pulse #85413 (figure 7), a deuterium-deuterium plasma with some residual hydrogen, all the deuterium channels appear to yield good signal, while only the lowest 4 hydrogen channels, representing energies between 4-13 keV, are reliable. As no tritium was present in the discharge, all the tritium channels likely show pure noise caused by sporadic neutron strikes or other false indications. After calibrating the measured counts based on the detector geometry and efficiency, the output of the diagnostic is the line-averaged energy spectrum of the neutral fluxes for each isotope (figure 8).

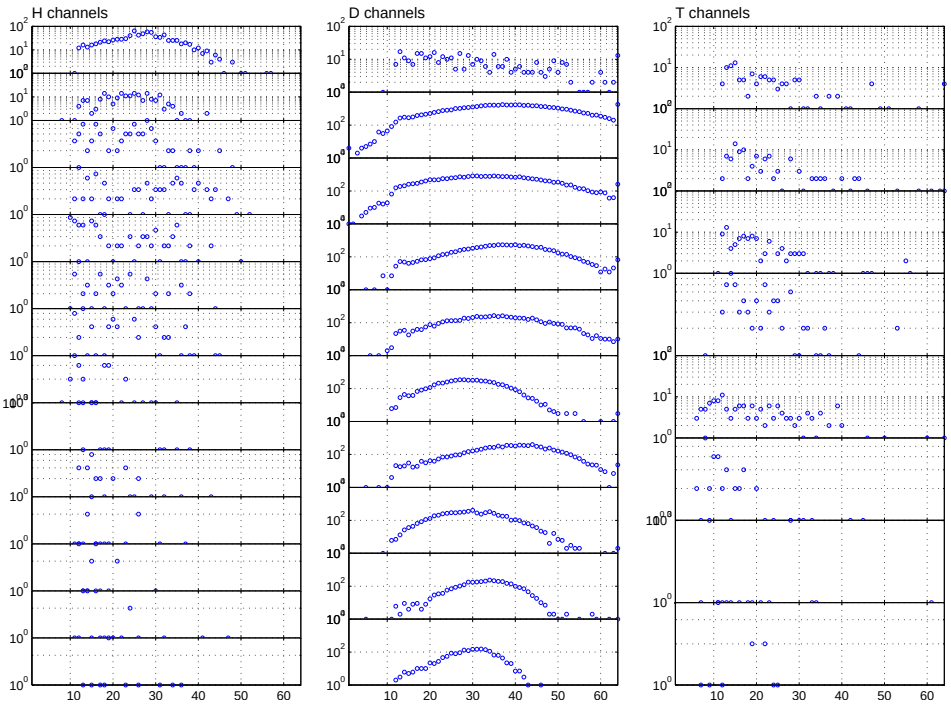

Figure 6: Raw counts in ADC bins for the JET pulse #85413, summed over the time slice 10-12 s into the pulse. Energy channels are laid out in the same order as in figure 7. Plotted using the JET kr2show utility. [16]

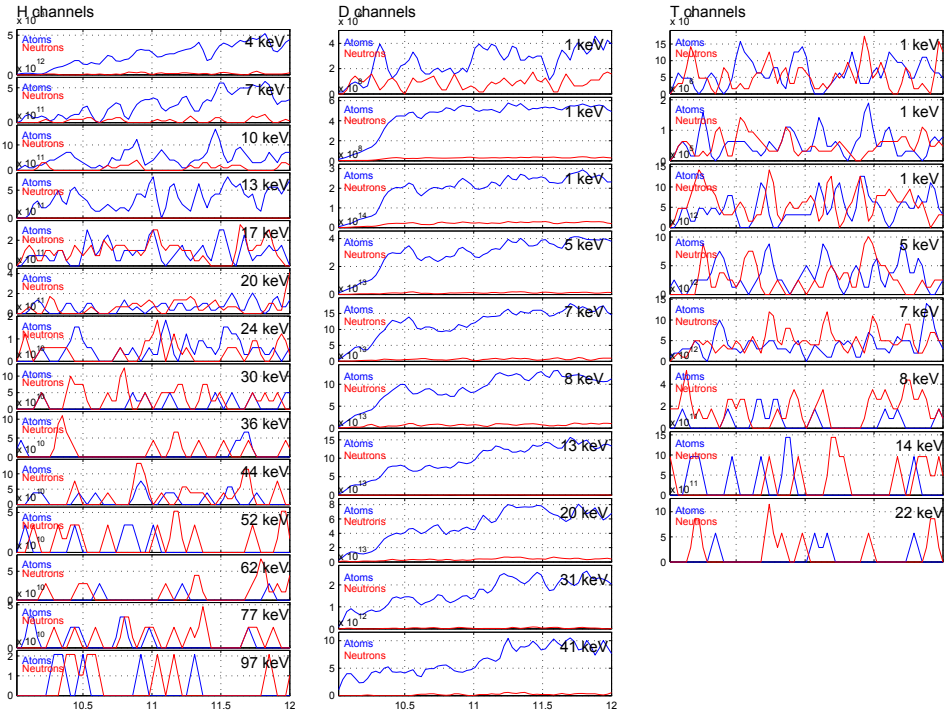

Figure 7: Time traces of neutral atom and neutron fluxes ($1/m^2$ s sr keV) for pulse #85413 during the time slice 10-12 s. Plotted using the kr2show utility.

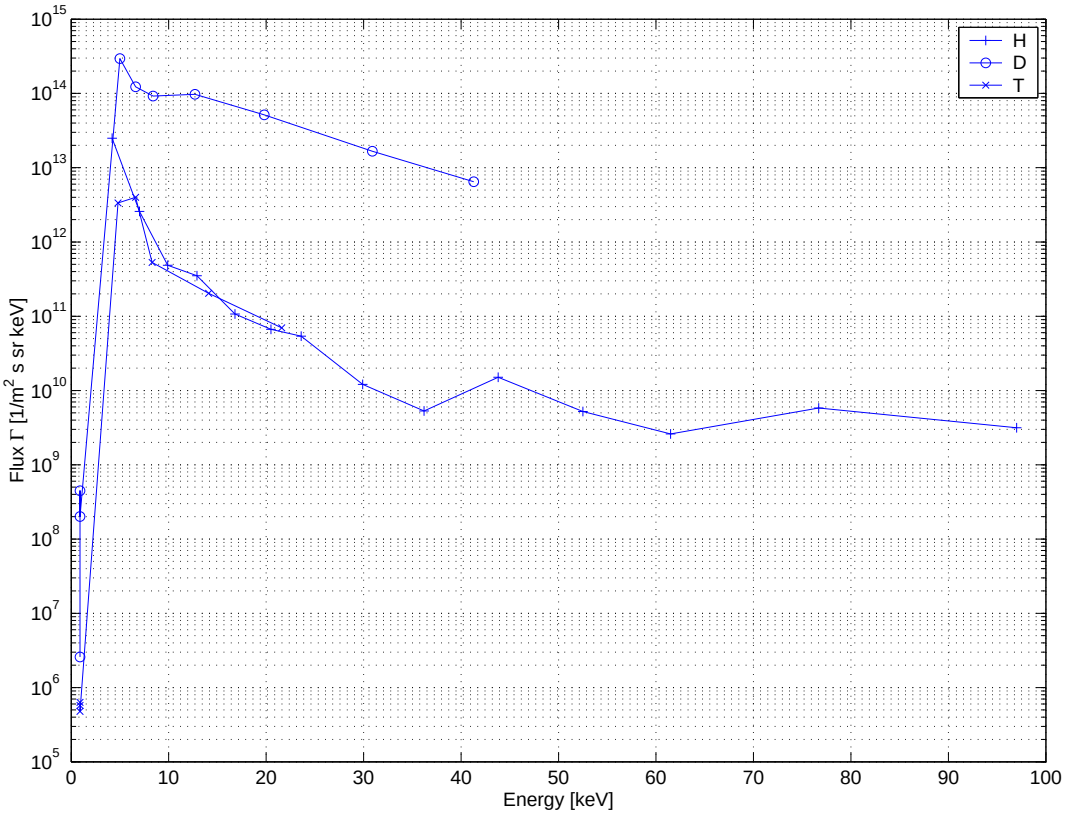

Figure 8: Line-averaged neutral particle fluxes for pulse #85413, averaged over time slice 10-12 s. Plotted using the JET kr2show utility.

3 Neutral particle sources

As discussed in the previous chapter, understanding the neutral particle sources is critical for analyzing the neutral particle emissions from the plasma ions. Neutrals are produced through various means both spontaneously as well as intentionally, and determining their non-uniform distribution in the plasma is critical for understanding the measured neutral fluxes.

The neutral sources in a tokamak plasma can be divided into three categories: the edge or recycling neutrals arising from interactions between the plasma and the tokamak wall, the beam neutrals intentionally injected into the plasma, and the spontaneously produced recombination neutral background. Each of these sources exhibits distinct spatial and energy distribution throughout the plasma.

3.1 Edge neutrals

Ions that escape the main plasma and hit the wall can be recycled back into the plasma through interactions with the material. They can be immediately reflected off the surface, typically picking up an electron from the wall material and re-entering the plasma as a neutral. The energy of the reflected neutral is some fraction of the incident energy, typically on the order of 0.1-1 keV. [2]

The impacting ion can also knock off, or sputter, other particles from the plasma surface. These particles can either be impurities, such as the wall material itself, or ions that have been deposited upon the wall. These particles are then ejected at an energy between the incident particle energy and the thermal energy of the material, approximately between 1-100 eV.

Finally, the particles can penetrate deeper into the wall, diffuse outwards and subsequently be desorbed from the wall typically as molecules. These neutrals have energies on the order of the thermal velocity of the particles in the wall, or 0.01-0.1 eV, but as they dissociate in the SOL the receive an additional 1-2 eV due to the dissociation energy.

The neutral particles leaving the wall penetrate ballistically into the plasma until they ionize, with the penetration depth dependent on their ejection energy and the plasma they encounter. The particles cannot penetrate very deep into the high density core plasma, resulting in a profile that is highly peaked near

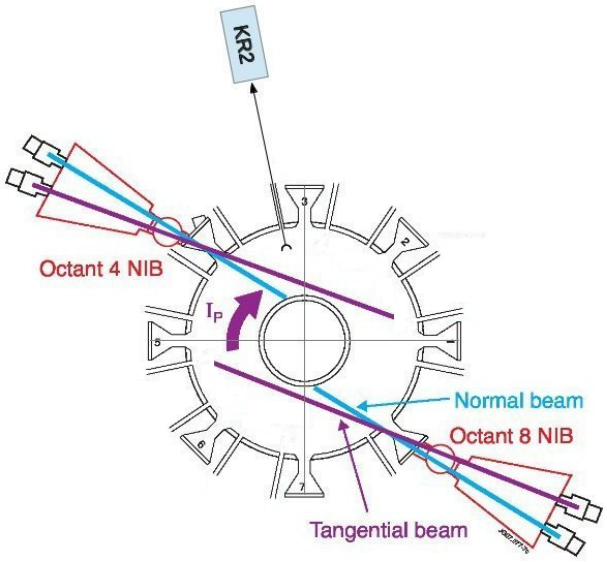

Figure 9: Layout of the neutral beams and the KR2 NPA diagnostic at JET.

the separatrix. Thus, in the edge region they can form the most significant source of neutrals for charge exchange reactions. [2]

3.2 Beam neutrals

Neutral particle injection (NBI) is another important source of neutral particles. High-energy neutral particles are fired into the plasma for heating and current drive purposes. Unlike the recycling neutrals, these fast particles can penetrate much deeper into the core, but their distribution is localized around the injection trajectory. Thus, they are only relevant for NPA if the detector sight line intersects the neutral beam.

3.2.1 Neutral beam injection

The neutral particle beams are created by first ionizing cold neutral gas, typically using arc discharges. The ions are then accelerated in an electric field generated by applying a voltage across successive accelerator grids through which the ions pass. The ions are then led into a neutralization chamber, where the beams are allowed to interact with a neutral gas through charge exchange reactions. The result is a beam of fast neutral particles which is then injected into the plasma.

At JET, the neutral beams are generated in two neutral injector boxes (NIBs) located at opposite sides of the torus. Each box contains 8 positive ion neutral

injectors (PINIs) in two columns. In each box, one column of beams is aimed in a radial direction towards the center of the device, and the other column is aimed in a more tangential direction with an oblique angle. Additionally, the PINIs are vertically aimed to converge as they enter the plasma. [17]

Each PINI can inject hydrogen, deuterium or tritium neutrals with a power of 2 MW and a maximum energy of 130 keV. However, due to molecular reactions involving two- and three-atom hydrogen molecules, a significant fraction of the injected particles only reach half or one-third of the maximum energy. [18] Each PINI can be switched on individually, enabling precise control of the power deposition depending on the heating and current drive needs.

The neutral particles penetrate ballistically into the plasma until they become ionized through charge-exchange and ionization reactions with the plasma ions and electrons, after which they following the magnetic field due to the Lorentz force, depositing their energy into the plasma through Coulomb collisions.

Since the neutral beam can be externally controlled by switching them on and off, neutral particle analysis using beam neutrals is called active NPA. However, this requires the beam trajectory to intersect the line of sight of the detector, and the plasma to be sufficiently transparent for the neutrals to reach the detector. For the JET beams, only the tangential beam of NIB 4 is within the KR2 NPA viewing cone.

3.2.2 Neutral halo

While the primary neutrals injected through NBI are lost during ionization, the reactions can result in secondary neutrals, since each ionization through charge exchange results in a new neutral particle. Unlike the primary neutrals, these have much lower energies, equivalent to the local ion temperature, and their velocity distribution is isotropic due to the Maxwellian background distribution. Thus they fly ballistically in arbitrary directions around the neutral beam and ionize much more rapidly than the primary neutrals due to their lower energy. Each successive ionization through CX can again result in a new neutral, until it is finally ionized through ion or electron impact.

These generations of secondary neutrals form a halo of neutral particles surrounding the primary neutrals in the beam. While they are slow and short-lived, they can contribute significantly to the neutral density. The number of suc-

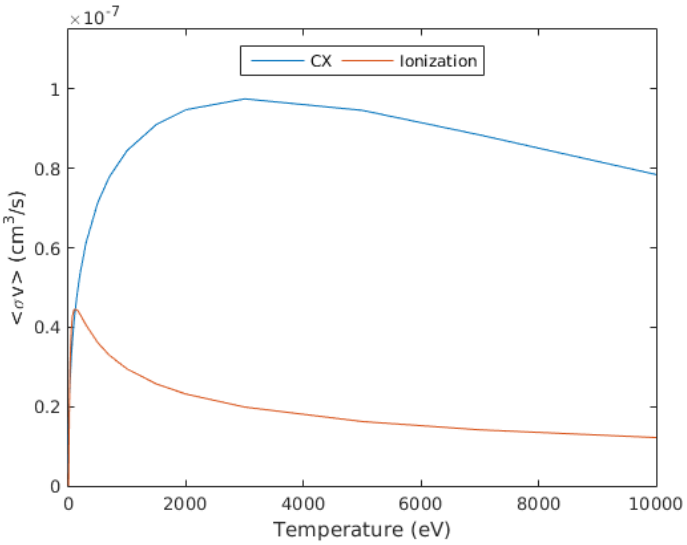

Figure 10: Charge exchange (blue) and ionization (red) rate coefficients as a function of plasma temperature. [12]

cessive charge exchanges depends on the ratio of cross sections for the CX and ionization reactions, which in turn depends on the plasma temperature (figure 10). For JET plasmas around 3 keV temperature, CX dominates with a rate coefficient 5 times higher than impact ionization. This means that only approximately 15-20% of neutrals are effectively lost in each successive generation.

The halo both increases the total neutral density in the vicinity of the beam as well as spreads out its distribution. This is especially important for active NPA, where the goal is to achieve high spatial resolution due to the tightly localized neutral distribution.

3.3 Recombination neutrals

The third source of neutral particles is the plasma itself, since it is a mixture of electrons and ions which can spontaneously recombine [19]. The neutrals are produced at a reaction rate proportional to the plasma density according to equation 4. The atoms have energies equal to the local thermal energy, and they penetrate ballistically in the plasma until they reionize through the ionization reactions. While the recombination neutrals are short-lived due to the high density in the core, this process results in a low but finite level of neutral density throughout the plasma.

4 Simulation tools

No single code exists for simulating all the interactions necessary to determine the various distributions of particles needed for predicting the neutral fluxes. Instead, multiple codes, each focused on a separate aspect of plasma simulation, must be combined and interfaced together.

The codes applied in this work are the orbit following code ASCOT, used for the fast ion simulations, the stand-alone synthetic NPA diagnostic ASCOT-NPA, the NBI ion deposition and neutral simulation code BBNBI and the edge plasma and neutral code suite EDGE2D-EIRENE.

4.1 ASCOT

ASCOT is a Monte Carlo orbit following code that solves the distribution of minority particles in a fusion plasma [20]. In this work the code was used to compute the slowing-down distribution of the NBI ions.

ASCOT follows an ensemble of test particles in an axisymmetric or 3D magnetic field either by following their full gyro orbits or guiding centers or by using a hybrid approach where full orbits are only followed near the wall. The slowing-down distribution is approximated by accumulating the particles in a 4D histogram.

The particles are followed until they slow down and thermalize or until they are lost. Collisions during the slowing down are modelled through a Fokker-Planck collision operator, and the particles are considered thermalized when they slow down to 1.5 times the local background ion temperature. The particles are considered lost when their trajectories intersect a wall, which can be defined either as a 2D limiter contour or an arbitrary 3D wall such as a detailed model based on CAD drawings of the device. [21]

4.2 ASCOT-NPA

ASCOT-NPA is a Monte Carlo -based synthetic diagnostic for neutral particle analysis originally written by Simppa Äkäslompolo [22]. The code can model the neutral particle emissions based on 1D neutral particle and plasma profiles and an arbitrary 4D ion distribution. Additionally, in this work an automatic

generation of a thermal bulk ion distribution based on the ASCOT 1D plasma profiles was implemented to model their contribution to the NPA signal.

The 4D distribution is given in the ASCOT HDF5 output format, which contains a discrete 4-dimensional histogram in the (R, z, ξ, E) space. For bulk plasma modelling, the axisymmetric 4D distribution is generated by sampling the plasma profiles at discrete radial locations and integrating the Maxwellian energy distribution

$$n_i(R, z, \xi, E) = n_{i0} 2 \sqrt{\frac{E}{\pi}} (kT_i)^{-3/2} e^{-\frac{E}{kT_i}} \tag{12}$$

where n_i is the ion density in the 4D distribution, n_{i0} is the ion density at the sampling location according to the plasma profiles, E is the energy and T_i the ion temperature. The integral is calculated using the Simpson rule [23] at discrete energy values between 0 and 50 keV, which is sufficient for most present fusion plasmas.

The diagnostic in ASCOT-NPA is represented by a viewing cone through which the neutral particles can enter and strike the detector. The cone is defined by giving the location of the apex, the location of one point along the sight line axis to determine the viewing direction, the opening angle of the cone and the area of the detector surface. The values used for the JET KR2 diagnostic are given in table 1.

The signal is integrated using the Monte Carlo method of randomly sampling (R,z) points in the poloidal region encompassing the viewing cone. The samples are weighted by the neutralization reaction rate at the location as calculated by equation 1. Each point is assumed to represent an equal fraction of the total volume of the viewing cone, which is a reasonable assumption when the cone is narrow.

Since the ion distribution can be highly nonisotropic, the ion density must be also be sampled in the velocity space. The pitch angle from the sample location to the detector is calculated as

$$\xi = \hat{b} \cdot \hat{r} \tag{13}$$

where $\hat{b}$ is a unit vector in the magnetic field direction and $\hat{r}$ is a unit vector from the sample location to the detector. The pitch values are calculated to

Table 1: ASCOT-NPA detector settings for the JET KR2 diagnostic

Viewing cone apex (x, y, z)	-12.465 m, -2.5359 m, 0.28 m
Sight line point (x, y, z)	-0.97992 m, -0.19937 m, 0.28 m
Viewing cone opening angle	0.015 rad
Detector surface area	7.29 mm^2

two points at the extreme extents of the detector surface. The ion density is then accumulated from the distribution only between these values ξ_{min} and ξ_{max}.

The fraction of particles at the sample location that can reach the detector is further limited by the gyro angle of the particles. Assuming the particles are uniformly distributed in the gyro angle space, the fraction of gyro angles reaching the detector is calculated through the fraction of full circle covered by the detector

$$\theta_{frac} = \frac{l}{2\pi r} \tag{14}$$

where l is the diameter of the detector and r is the distance from the sample location to the detector. For large r this corresponds to the fraction of the viewing angle of the detector from the gyro orbit of the particle.

After determining the neutral source, the neutral signal is attenuated as it passes through the plasma. The attenuation factor is computed by numerically integrating the neutral attenuation in equation 10 using the QUADPACK library [24]. The signal computed in the previous step is then multiplied by this factor.

Finally, the attenuated neutral rate is normalized by the detector area A and the solid angle of the detector viewing cone Ω to determine to flux of particles to the detector. The fluxes are calculated for each discrete energy value in the 4D distribution.

The convergence of the algorithm was studied by repeating a simulation with increasing number of sample locations using a representative NBI ion distribution and the KR2 geometry (figure 11). Beyond 10^6 Monte Carlo samples the results remain within 15% of the more precise values, and within 2% for 10^7 samples. The simulations in this work were performed with 10^6 samples.

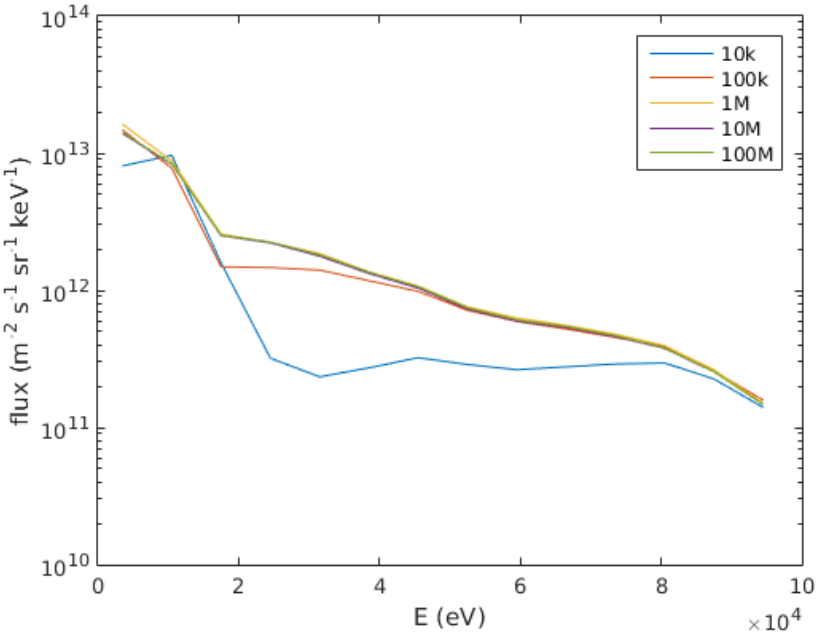

Figure 11: Convergence of the NPA algorithm. The simulation was repeated with increasing number of Monte Carlo sampling points.

4.3 BBNBI

BBNBI is a Monte Carlo code that solves the NBI ion source distribution by following beam neutrals from the injector until ionization [26]. In this work, the code was extended to also compute the 3D neutral density of the injected particles.

The injector model in BBNBI is defined as a set of beamlets representing the actual geometry of the last accelerator grid in the injector. Each beamlet is individually focused, and a circular symmetric divergence of the particle beam can be specified. Additionally, the probabilities for different energy and isotope fractions can be given.

The code can use two different sources for the effective ionization probabilities, called beam stopping coefficients. The first is the Suzuki model which is an analytic fit to experimental measurements [27]. The second is a model interpolated from experimental data in the ADAS database [12]. While more comprehensive, with coefficients for hydrogen and helium beams in various plasmas and impurity species, the ADAS library is presently only available at the JET analysis cluster (JAC), limiting the available platforms for running the simulations. The JET simulations presented here were performed using the ADAS library.

BBNBI initializes neutral particles at each beamlet based on the isotope, energy and divergence probability distributions. The ballistic trajectories of the particles are followed with adaptive step sizes and the attenuation in equation 2 is integrated along this trajectory until it reaches a predetermined random value, at which point the neutral is considered ionized. If the particle completely penetrates the plasma and impacts the wall it is considered to be shine-through. Finally, the weights of the particles are normalized to the injector power setting. The particles are then written out in the ASCOT particle input format. BBNBI can set up the NBI injector configuration either automatically by importing the energies and powers from JET PPF files or by manually setting the values for each injector.

The 3D neutral distributions are computed by accumulating the neutral particles in a 3D histogram after each time step. The contribution is calculated as

$$dn = w\frac{ds}{v}, \tag{15}$$

where w is the weight of the particle, v is the velocity, ds is the distance travelled in one time step. After the simulation the density is obtained by dividing the number of particles in each histogram bin by the bin volume.

4.4 EDGE2D-EIRENE

EDGE2D-EIRENE [28] is an integrated code for simulating plasma and neutral particles near the edge of the plasma and the wall. The code consists of EDGE2D [29], a two-dimensional magnetohydrodynamic (MHD) code that computes the dynamics of the plasma in a fluid approximation, and EIRENE [30], a 3D Monte Carlo code for following neutral particles.

The code works by alternating the two codes and iterating the process until a self-consistent solution is found. EDGE2D solves the Braginskii fluid equations that describe the evolution of the plasma densities and flows on a two dimensional grid encompassing the scrape-off layer. Neutral particle sources from EDGE2D are then passed on to EIRENE, which solves the neutral distribution by following the trajectories of neutrals until they are ionized. The ions then act as sources in the EDGE2D code.

5 Neutral particle analysis of JET NBI ions

To study the feasibility of using NPA for diagnosing the NBI ions, ASCOT-NPA was applied, together with the support from the other codes, to simulate the neutral emissions in a suitable JET discharge. Additionally, two cases with full NBI power and varying density were simulated to study the effect of different injector configurations on the neutral flux.

The first section describes the plasma equilibrium and profiles used in the simulations. In the second and third sections, the fast ion and neutral distributions in the studied cases are discussed. Finally, the fourth and fifth section present the neutral particle fluxes as simulated for NBI and bulk plasma ions.

5.1 Equilibrium and plasma profiles

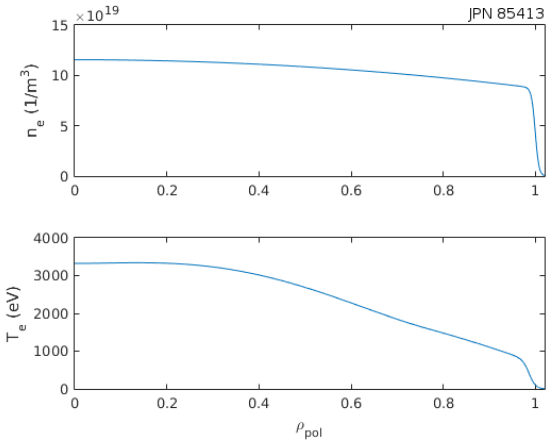

Figure 12: Fitted electron density (top) and temperature (bottom) profiles for the JET pulse #85413 at 11-12 s.

The plasma equilibrium and profiles used in the study are based on JET pulse #85413. The choice of discharge was limited by several factors. Firstly, ASCOT can presently only model the distribution of NBI ions. Other heating methods such as ion cyclotron heating (ICRH), commonly used in high-performance plasmas, further modify the energy distribution of the plasma ions, which can itself mask the effect of NBI heating. Secondly, the precise neutral distribution calculations with EDGE2D-EIRENE are very time-consuming. For that reason only pulses for which the necessary neutral simulations had already been performed were considered, in this case provided by Aaro Järvinen [31]. Finally,

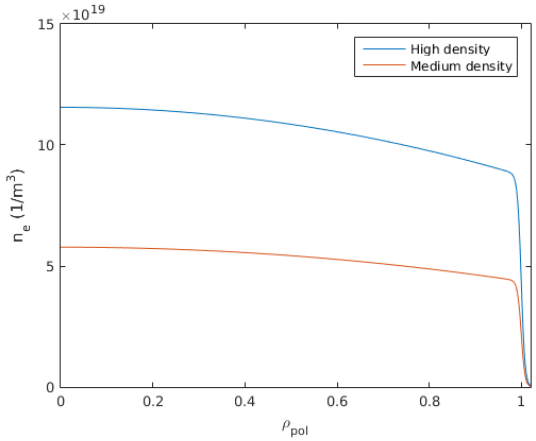

Figure 13: Plasma density profiles for the studied high and medium density cases.

KR2 NPA measurements were not available for every pulse, further narrowing down the choice of discharges.

The studied discharge features a high-density, high confinement mode (H-mode) plasma with heavy nitrogen injection, with core density of $9 \cdot 10^{19}$ $1/\mathrm{m}^3$ and temperature of 3 keV (figure 12). Initial studies were performed directly using profiles measured with high resolution Thompson scattering (HRTS), but the profile near the edge, critical for determining NBI deposition, was found to be inaccurate. Instead, fitted profiles prepared by Dr Matthew Leyland of York University were used. As required for ASCOT modelling, no ICRH heating was used in the pulse until shortly before the end of the discharge. NBI power was applied between 10-15 s with an injection energy of 120 keV and a total power of 20 MW. The time slice studied was selected in the middle of the NBI heating between 11-12 s into the pulse.

To study the effect of different NBI injectors on the signal more carefully, two conceptual cases were also modelled (figure 13), with plasma profiles scaled from the ones in #85413. The high density case assumed a core density of $9 \cdot 10^{19}$ m^{-3}, while the medium density case assumed the density to be reduced by 50% to $5 \cdot 10^{19}$ m^{-3}. Edge and recombination neutral densities were scaled similarly by 50%. In both cases full NBI power from each injector was applied and modelled separately.

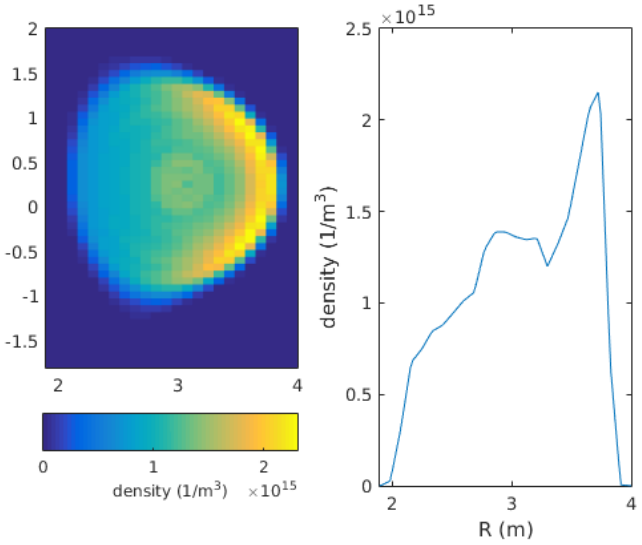

Figure 14: ASCOT-simulated NBI ion slowing-down density in the poloidal plane (left) and along the NPA sight line (right).

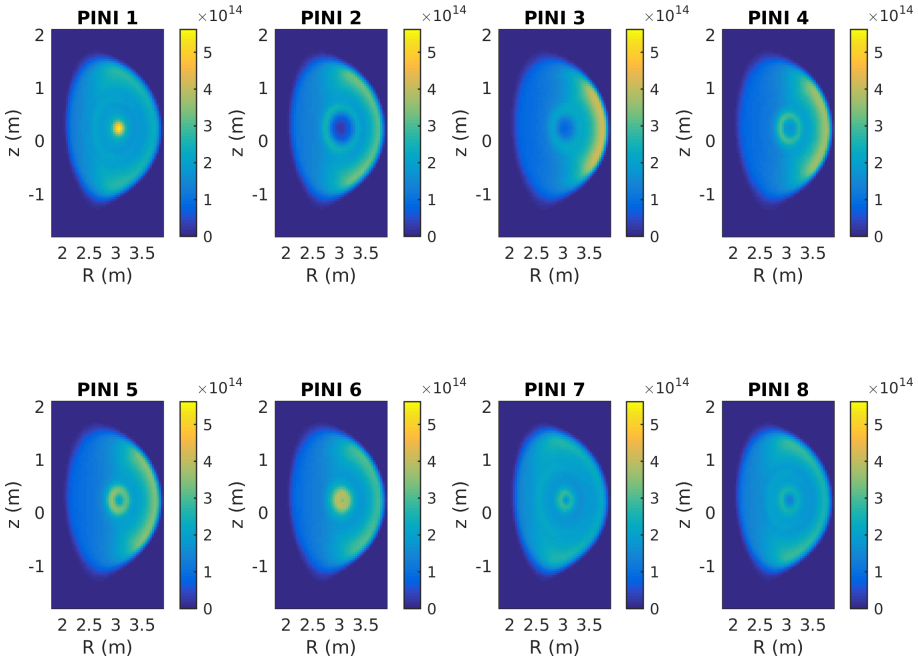

Figure 15: NBI ion slowing-down densities for individual PINIs of NIB 4 in the high density case. NIB 8 PINIs are identical due to symmetry.

5.2 Fast ion distributions

The NBI ion slowing-down distribution in pulse #85413, as calculated by ASCOT, exhibits a profile that is peaked near the low field side edge (figure 14). This is due to the high plasma density and steep pedestal gradient, which prevent the beam neutrals from penetrating deep into the plasma. Instead they are ionized fairly close to the separatrix onto banana orbits that remain near the edge.

In the assumed high density case, otherwise identical to the plasma in pulse #85413, the radial injectors 3, 4, 5 and 6 have significant NBI slowing-down density near the edge due to their banana orbits, whereas the tangential injectors 1, 2, 7 and 8 have a more uniform distribution (figure 15). In the assumed medium density case, corresponding to an H-mode at half the density of #85413, the beams are able to penetrate much deeper into the plasma, and the densities are peaked closer to the center of the plasma for each injector (figure 16).

In the reference pulse and the assumed high-density case, it is important to notice that the distribution of the ions is very sharply peaked near the edge. Because the neutral distribution near the edge also is highly peaked, this means that the distributions must be resolved at high spatial accuracy, since

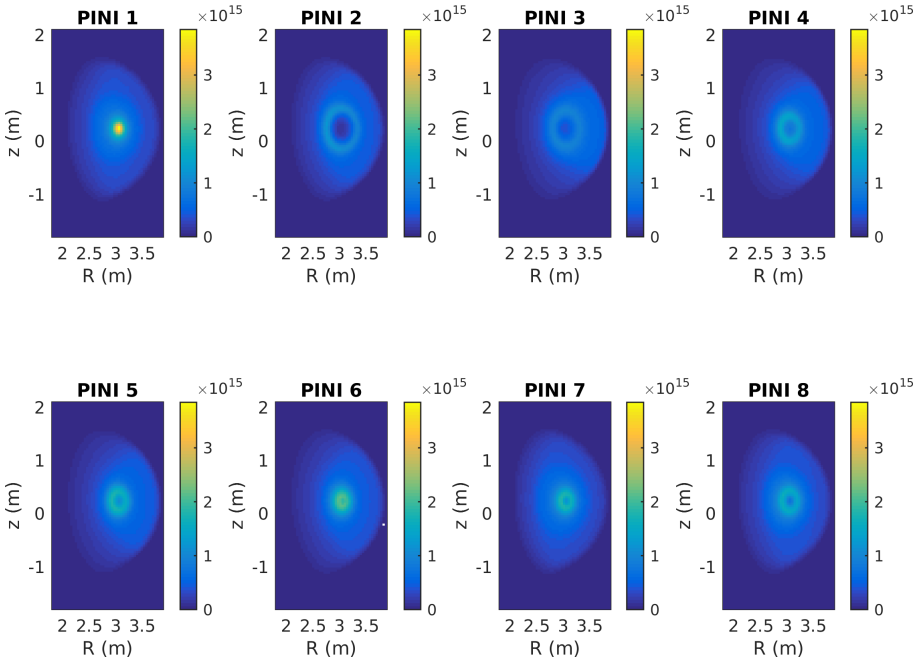

Figure 16: NBI ion slowing-down densities for individual PINIs of NIB 4 in the medium density case.

small changes in the location of the peak can change the signal, which is a product of the two, by orders of magnitude. The standard ASCOT fast ion distributions, with a grid of 25x50 spatial bins for the entire plasma, were found to be completely inadequate for the NPA studies. Instead, the distributions were only computed in a narrow region around the NPA sight line, with 200x20 spatial bins.

5.3 Neutral densities

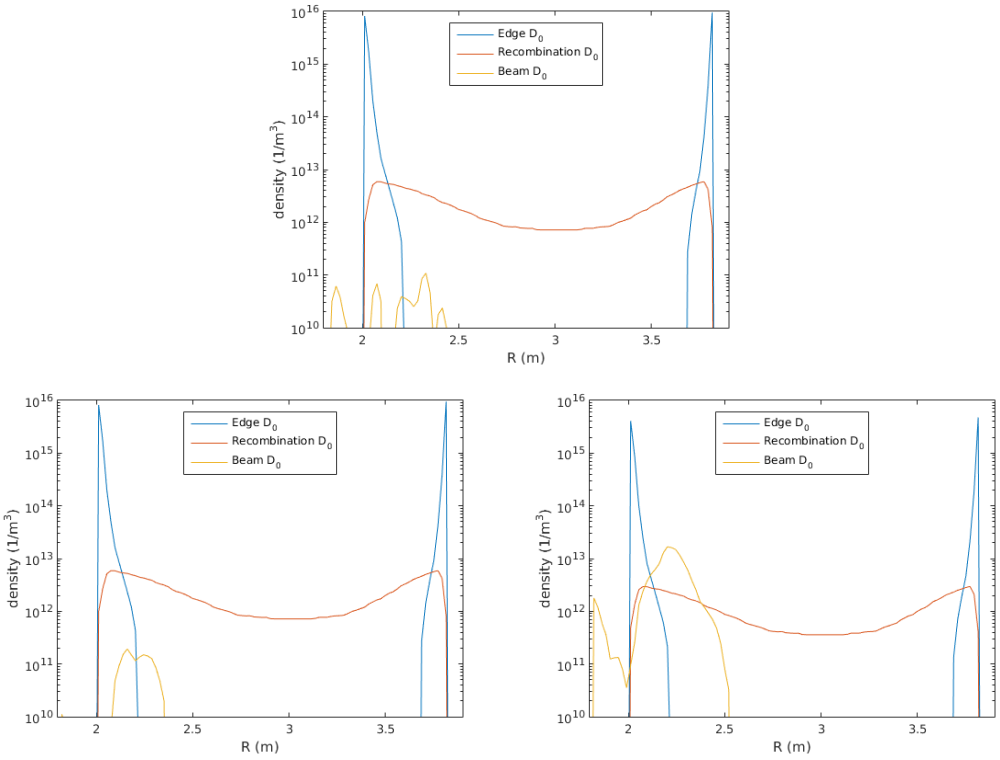

Figure 17: ASCOT, EDGE2D-EIRENE and BBNBI predicted edge, recombination and NBI neutral densities, respectively, along the NPA sight line for pulse #85413 (top), high density (bottom left) and medium density (bottom right) cases.

In all the studied cases, the neutral density profile is dominated by sharply peaked recycling neutrals near the edge of the plasma (figure 17). The edge density is up to three orders of magnitude higher compared to the recombination neutrals inside the plasma. However, the recombination neutrals provide a nearly constant source for charge exchange reactions throughout the plasma. The edge and recombination neutral densities are identical in the reference and assumed high density cases. For the assumed medium density case, they were reduced by 50% with the assumption that they would approximately scale linearly with the plasma density that acts as the source for these neutrals.

In pulse #85413 and the assumed high density cases, the NBI neutral density was found to be insignificant compared to the other sources. This is due to the combination of high density and the NBI injector geometry (figure 9). In order to reach the NPA sight line to generate a detectable neutral flux, the neutrals

of the tangential beam must fully penetrate the core to the opposite side of the plasma. Because of the high density, however, most of the neutrals are ionized soon after leaving the injector (figure 18). For this reason very few neutrals enter the detector's viewing cone.

Because the neutrals do not ionize as strongly in the assumed reduced density of the medium density case, a significant fraction of them can reach the opposite side of the plasma and cross the detector sight line. This results in a localized neutral density on the sight line that would exceed even the full recombination neutral density (figure 17, bottom right). However, the particles neutralized in this region must penetrate back through the dense core in order to reach the NPA detector and be measured. Furthermore, the energy of these neutrals, resulting from charge exchanges with thermal and slowing-down beam ions, is lower than that of the original beam, which means the neutral flux will rapidly attenuate in the plasma.

For the aforementioned reasons, the beam neutral densities were deemed insignificant for the measured neutral fluxes and were not included in the neutral density profiles in the simulations.

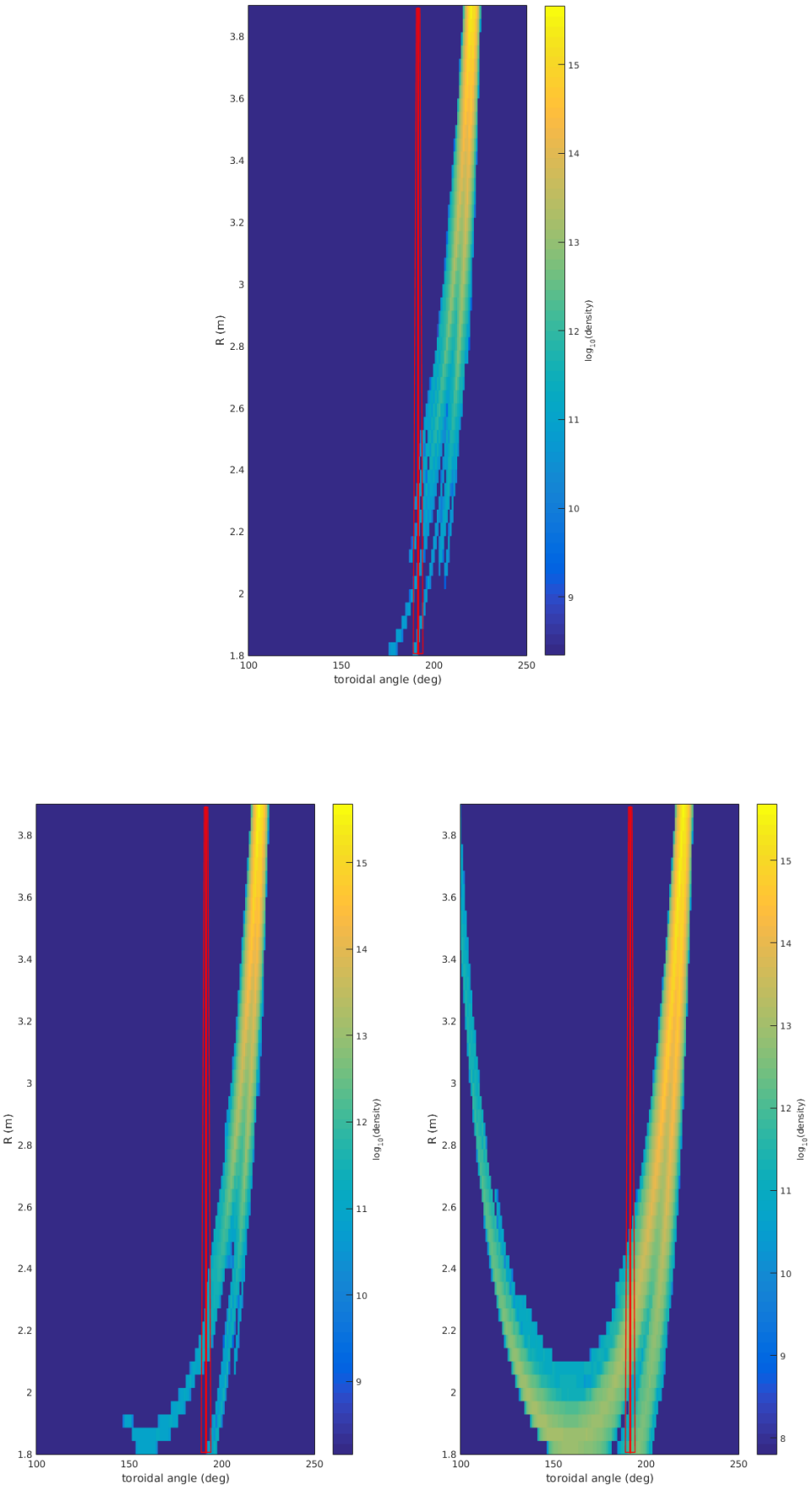

Figure 18: Mean beam neutral densities for pulse #85413 (top), high density (bottom left) and medium density (bottom right) cases with the NPA viewing cone indicated in red.

5.4 Synthetic NPA for NBI ions

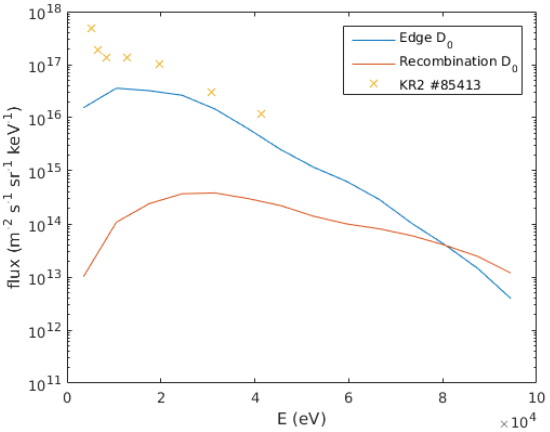

Figure 19: ASCOT-NPA simulated NBI neutral fluxes for pulse #85413 using only the edge or recombination neutral densities together with the measured signal.

As expected based on both the fast ion and the neutral distributions presented above, the simulated NPA signal is dominated by the edge neutrals (figure 19). Their contribution is more than one order of magnitude greater than that of the recombination neutrals nearly throughout the energy range of the slowing-down NBI ions. Only at energies beyond 80 keV, corresponding to the full NBI energy, does the recombination neutral contribution exceed the edge neutral contribution. This is likely due to the highest energy ions being localized further inwards from the edge neutral dominated region, where the high temperature and resulting low collisionality result in longer slowing-down times for the beam ions.

The simulated neutral flux for the NBI ions appears to follow the measured signal at higher energies, suggesting both a qualitatively correct model as well as fairly realistic neutral profiles. However, the signal is predicted to fall off at energies below 20 keV, which suggests the presence of another source of neutral flux in the low energy region.

Since the edge neutral density was deemed to be critical for the NBI neutral flux, the effect of changing the shape of this profile was studied in more detail. By uniformly scaling the edge neutral profile, the simulated neutral flux was found to scale approximately linearly with the neutral profile (figure 20). This is the expected result, as the neutral flux integral in equation 11 depends linearly on the neutral density.

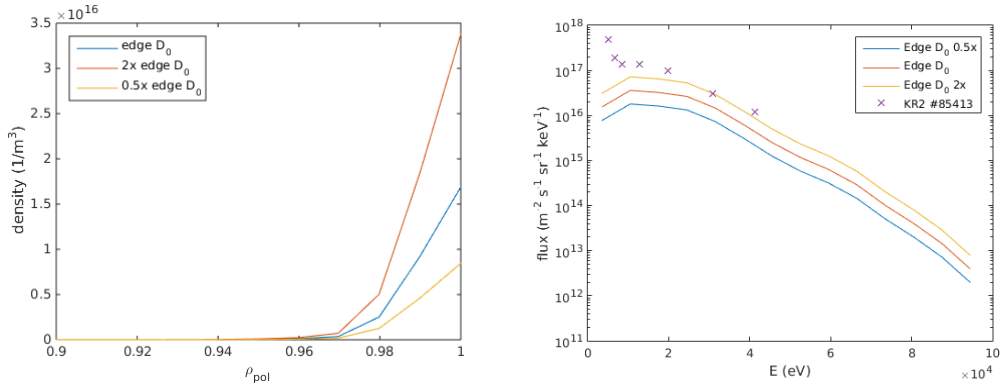

Figure 20: Simulated NBI neutral fluxes for pulse #85413 (right) using scaled edge neutral densities (left) with the measured signal.

Physically, scaling the density of the neutrals is equivalent to adjusting the total amount of recycling neutrals emitted from the walls. As the recycling neutrals originate from the bulk plasma, the level of recycling neutrals would likely depend strongly on the plasma density, although other factors such as conditions in the scrape-off layer may also affect the recycling.

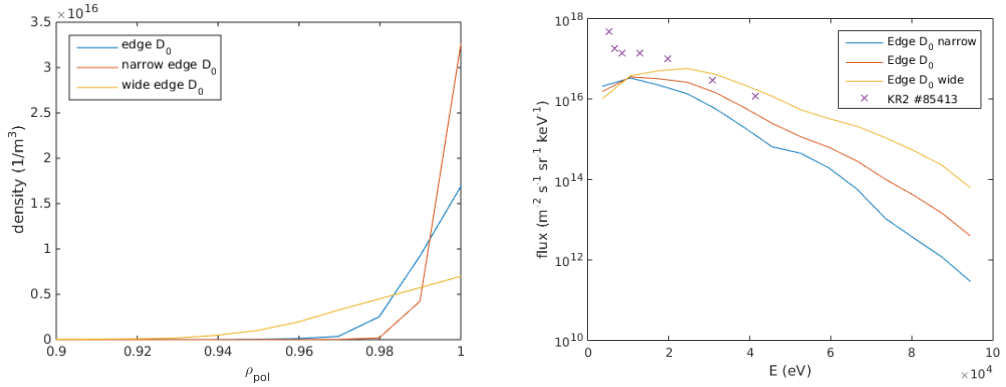

Figure 21: Simulated NBI neutral fluxes for pulse #85413 (right) using narrowed and widened edge neutral density profiles (left) with the measured signal.

In contrast, adjusting the width of the edge neutral density, while keeping the total neutral density approximately constant, has a greater effect on the high-energy neutral flux (figure 21). The wide profile, introducing a greater neutral density deeper in the plasma, corresponds to an increased high-energy flux. This would be consistent with the aforementioned observation that the high-energy ions reside further away from the edge.

Scaling the width of the neutral density has the physical equivalent of changing the energy of the recycling neutrals ejected from the wall, as higher energy

neutrals will be able to penetrate deeper into the plasma. The energy would likely depend on the plasma temperature, affecting both the energy of recycled neutrals as well as the temperature of the wall.

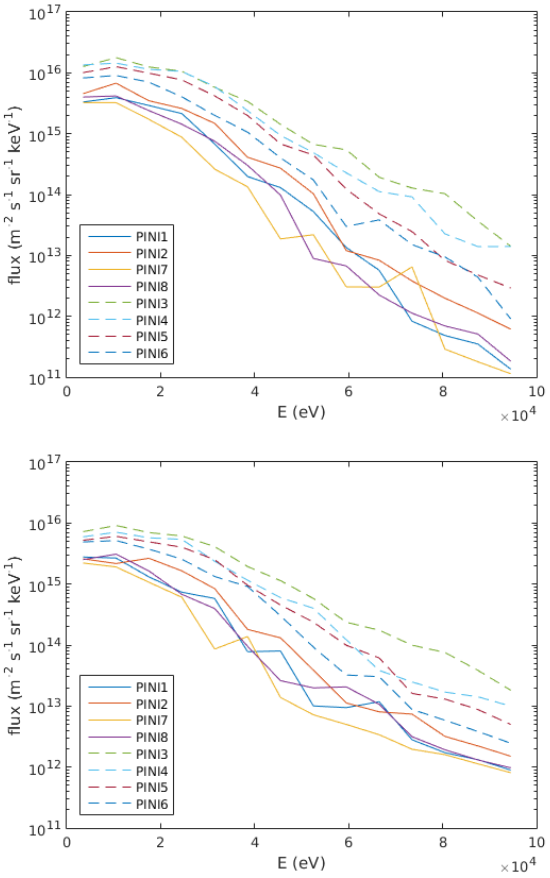

Figure 22: Neutral fluxes from individual injectors in the high density (top) and medium density (bottom) cases. PINIs 1, 2, 7 and 8 form the tangential beams, PINIs 3, 4, 5 and 6 the radial injector beams.

To study the effect of different NBI PINI configurations on the NPA signal, the neutral flux was simulated individually for each of the 8 PINIs in injector box 4 in the high and medium density cases using the fast ion profiles shown previously. In both cases, the radial beams from PINIs 3-6 result in higher neutral fluxes compared to the tangential beams from PINIs 1, 2, 7 and 8 (figure 22). This is likely due to the velocity space distribution of the ions, which for the perpendicularly injected radial beams has correspondingly larger perpendicular velocities and thus smaller pitch angles. As the NPA sight line is also perpendicular to the magnetic field, only the neutrals resulting from low pitch particles can reach the detector.

The noise in the simulated fluxes for the individual injectors is not due to the Monte Carlo integration of the neutral flux, but rather results from noise in the fast ion distributions as calculated by ASCOT. While the 10^5 test particles used in simulating the individual distributions are sufficient for the standard distribution resolution, the increased resolution used for the NPA studies would require better statistics with a larger number of test particles. This is evident in the smoother fluxes in figures 20 and 21 where a total of 10^6 test particles were used.

5.5 Synthetic NPA for bulk plasma

The neutral flux from the bulk plasma ions (figure 23), simulated using a thermal 4D distribution computed by ASCOT-NPA from the 1D plasma profiles, exhibits markedly different behaviour from the NBI neutral flux (figure 19). The bulk neutral flux is peaked at the lowest energies, where it is orders of magnitude higher than the beam neutral flux. Additionally, the recombination neutral contribution exceeds the edge neutrals already at the energy of 10 keV. This is due to the temperature of plasma increasing towards the center of the plasma. Thus the recombination neutrals cannot be disregarded for the bulk plasma simulations.

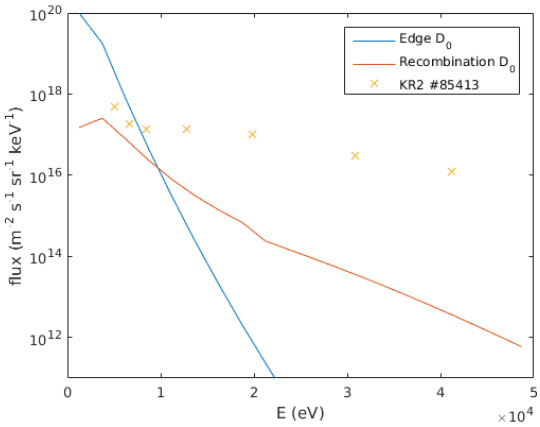

Figure 23: Simulated bulk neutral flux for pulse #85413 using only the edge or recombination neutral densities together with the measured signal.

Combining the simulated neutral fluxes from both NBI and bulk plasmas, adding both the effect of the edge and recombination neutrals, a total neutral flux can be represented (figure 24). The highest energies are again within a factor of two of the measured fluxes. However, between 10-20 keV the simulated signal falls off too rapidly. Based on the edge neutral scaling simulations, this may be due to too low and broad edge neutral density. Alternatively, a higher core recombination neutral density could increase the bulk neutral signal in this energy range.

For energies below 10 keV, where the bulk neutral flux dominates, the simulation overestimates the total flux by one order of magnitude. This could be due to excessive neutral density in the low temperature region near the edge, either due to recycling neutrals penetrating too deep or due to overestimated recombination neutral density.

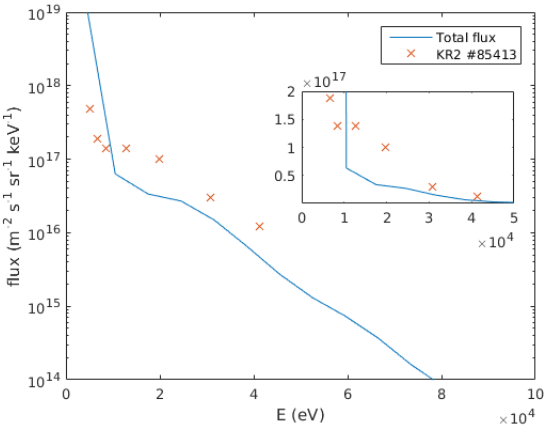

Figure 24: Total simulated neutral flux with the measured signal. Inset shows the plot on linear scale.

6 Summary and conclusion

Neutral particle analysis is a method for diagnosing ions in a tokamak plasma by measuring the flux of emitted neutral particles. In this thesis, numerical simulations were used to model the neutral flux resulting from energetic NBI ions. A suite of codes, including the synthetic diagnostic ASCOT-NPA, the fast ion orbit following code ASCOT, the NBI ionization code BBNBI and the neutral particle code EIRENE, were used the simulate fast ion and neutral particle distributions and the resulting neutral fluxes.

Several neutral particle sources, acting as sources for charge exchange reactions emitting the measured energetic neutral fluxes, were identified and their relative importance was assessed. The most significant neutral source was determined to be recycling neutrals entering the core plasma from the walls. Their profile is peaked near the edge of the plasma, which means the measured neutral flux also primarily represents the ions in the edge region. Neutrals resulting from recombination of electrons and ions throughout the plasma were determined to be a significant contributor to the neutral signal from the core plasma. Primarily due to the geometry of the JET neutral beams and the NPA diagnostic, beam neutrals themselves were determined to have only a small effect on the neutral flux.

The simulated neutral particle flux was found to be very sensitive to the fast ion and neutral profiles, as both are strongly peaked near the edge of the plasma. The overall neutral density has an effect of scaling the resulting neutral flux, but the shape of the neutral profile, dependent on the energy of the incoming neutrals, strongly affects the shape of the simulated neutral flux.

In addition to the plasma and neutral profiles, the fast ion source was found to significantly affect the neutral flux. Radial NBI injection was predicted to result in a higher measured flux likely due to the higher perpendicular velocity of the injected particles compared to tangential injection. Additionally, each injector produced subtly different fast ion distributions, resulting in different neutral fluxes.

By combining the results of the simulations for both the bulk and NBI ions, using both the recycling and recombination neutral sources, the qualitative behaviour of the measured neutral flux in JET pulse #85413 could be reproduced. Differences were observed in the 10-20 keV energy range for the NBI ions, as

well as in the 5-10 keV range for the bulk ions, where their neutral signal was strongly overestimated. These discrepancies could possibly be explained with our inability to accurately determine the neutral profiles.

The results indicate that neutral particle analysis of NBI ions at JET is a feasible and promising diagnostic method. However, the strong dependence on the neutral profiles requires detailed, robust and comprehensive numerical modelling to obtain reliable results.

The recycling neutral density needs to be modelled in detailed for each pulse that is simulated, or a robust method for scaling the density based on the plasma scenario should be obtained. The EDGE2D-EIRENE simulations have the advantage of producing a self-consistent solution that can be validated against the plasma profiles. However, these simulations are lengthy, and obtaining consistent results requires detailed analysis and understanding. A simpler neutral model, such as using a stand-alone neutral code such as EIRENE or FRANTIC, would be an option, assuming the recycling rate of neutrals can be determined with sufficient accuracy.

The recombination neutrals, important for the bulk plasma simulation, need to also be modelled in detail. The simple scaled core neutral density model used here is not representative of plasmas with varying temperature profiles, altering the shape of the neutral density profile due to varying ionization rates. A neutral code capable of simulating the neutral profile throughout the plasma should be used for this task.

Simulating the relevant atomic reactions both during neutral density as well as neutral flux calculations require accurate cross section data. While the ASCOT family of codes already uses ADAS data in some computations, a comprehensive implementation of atomic reactions using the ADAS library would make the codes simpler and more consistent with each other. The limited availability of the ADAS library is also an issue, as some of the computations in this work greatly exceed the typical requirements of ASCOT simulations on the JET analysis cluster. This could be also be alleviated by optimizing the codes.

Once the ASCOT-NPA model is robustly validated against a wide range of plasma scenarios, it can be applied to interpretative and predictive simulations at JET. Depending on the confidence in the fast ion and neutral profiles, the model could alternatively be used to diagnose either distribution. Fixing the fast ion distribution with other diagnostics such as neutron diagnostics

or spectroscopy would enable analysis of the neutral distribution, and vice versa if the neutral profiles could be experimentally fixed for example using spectroscopy near the edge.

For measuring the isotope ratios, the results presented here yield ambiguous conclusions. Diagnosing the isotope ratio of the beam ions themselves should be straightforward from the high-energy fluxes, which almost exclusively correspond to the fast ion density. However, the shape of the neutral flux is strongly affected by the neutral profiles, and the resulting uncertainty could negate any advantage in unmasking the bulk neutral signal. The lowest energy channels are dominated by the bulk plasma neutral flux, enabling their use in isotope ratio measurements. Depending on the neutral profiles this analysis could be limited to the edge of the plasma where the recycling neutrals dominate.

References

[1] Tokamak principle. EUROfusion, https://www.euro-fusion.org/

[2] Wesson J., Tokamaks. Oxford University Press, 2004.

[3] Thomas P. R. et.al., Observation of alpha heating in JET DT plasmas. Physical review letters 80(25), 1998.

[4] Skinner C. H. et.al., Tritium diagnostics by Balmer-alpha emission. Plasma Physics Laboratory, Princeton University, Technical report, 1993.

[5] Hillis D.L. et.al., Tritium concentration measurements in the Joint European Torus divertor by optical spectroscopy of a Penning discharge. Review of Scientific Instruments 70(1), 1999.

[6] Maas A.C. et.al., Diagnostic Experience during Deuterium-Tritium Experiments in JET, Techniques and Measurements. JET–P(98)80, 1999.

[7] Bracco G., Guenther K., H/D Measurement by Neutral Particle Analysis at JET. JET-R(96)04, 1996.

[8] Bettella D. et.al., First measurements on the core and edge isotope composition using the JET isotope separator neutral particle analyser. Plasma Physics and Controlled Fusion 45(10), 2003.

[9] Kurki-Suonio T. et.al., Edge Fast Ion Distribution - benchmarking ASCOT against experimental NPA data on ASDEX Upgrade. In 33rd EPS Conference on Plasma Physics, Rome, Italy, 2006.

[10] Jämsä S. et.al., Benchmarking the fully 3D ASCOT-code against experimental NPA data from ASDEX Upgrade. In 36th EPS Conference on Plasma Physics, Sofia, Bulgaria, 2009.

[11] Hirvijoki E., Assessment of the performance of active NPA design in ASDEX Upgrade tokamak using the ASCOT code. Master thesis, Aalto University, 2010.

[12] ADAS Atomic Data and Analysis Structure, http://www.adas.ac.uk.

[13] Unterberg B., Transport Processes in the Plasma Edge. Proceedings of the Tenth Carolus Magnus Summer School on Plasma and Fusion Energy Physics, Fusion Science and Technology 61(2T):199-212, 2012.

[14] Afanasyev V. I. et.al., Neutral particle analyzer/isotope separator for measurement of hydrogen isotope composition of JET plasmas. Review of Scientific Instruments 74(4), 2003.

[15] Santala M., Custom Silicon Detectors To Enhance Jet Neutral Particle Analysers For Dt Operations. Proceedings of the 1st EPS conference on Plasma Diagnostics, Frascati, Italy, 2015.

[16] Private communication with Marko Santala.

[17] G. Duesing et.al., Neutral Beam Injection System. Fusion Science and Technology 11(1), 1987.

[18] Ciric D. et.al., Performance of upgraded JET neutral beam injectors. Fusion Engineering and Design 86(6-8), 2011.

[19] Dnestrovskij Y. N. et.al., Recombination-induced neutral particle flux in tokamaks. Nuclear Fusion 19(3), 1979.

[20] Hirvijoki E. et.al., ASCOT: Solving the kinetic equation of minority particle species in tokamak plasmas. Computer Physics Communications 185, 2014.

[21] Äkäslompolo S., Fast ion simulations in toroidally asymmetric tokamaks - Model validation with fast ion probes at ASDEX Upgrade and predictive modelling of ITER. Doctoral dissertation, Aalto University, 2016.

[22] Private communication with Simppa Äkäslompolo.

[23] Press W. et.al., Numerical Recipes in Fortran, 2nd Edition. Cambridge University Press, 1992.

[24] Piessens R., De Doncker-Kapenga E., Überhuber C.W., QUADPACK: a subroutine package for automatic integration. Springer, 1983.

[25] Atomic and Plasma-Material Interaction Data for Fusion, Volume 4. IAEA, 1993.

[26] Asunta O. et.al., Modelling neutral beams in fusion devices: Beamlet-based model for fast particle simulations. Computer Physics Communications 188, 2015.

[27] Suzuki, T. et.al., Attenuation of high-energy neutral hydrogen beams in high-density plasmas, Plasma Physics and Controlled Fusion 40(12) 2097–2111, 1998.

[28] Wiesen S., EDGE2D/EIRENE code interface. 2006.

[29] R. Simonini et.al., Models and Numerics in the Multi-Fluid 2-D Edge Plasma Code EDGE2D/U. Contributions to Plasma Physics 34(2-3), 1994.

[30] Reiter D., The EIRENE Code User Manual. 11/2009.

[31] Järvinen A., Radiative divertor studies in JET high confinement mode plasmas. Doctoral dissertation, Aalto University, 2015.